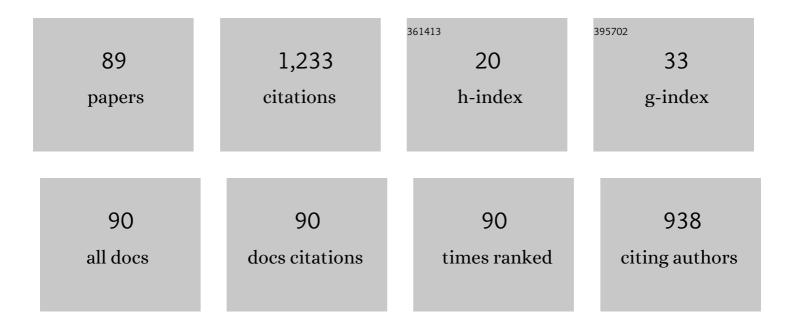
Emmanuel Dinnat

List of Publications by Year in descending order

Source: https://exaly.com/author-pdf/1917998/publications.pdf Version: 2024-02-01



#	Article	IF	CITATIONS
1	Sensitivity of Wide Bandwidth Radiometer for Remote Sensing of Ocean Salinity. IEEE Transactions on Geoscience and Remote Sensing, 2022, 60, 1-17.	6.3	3
2	Measurement of SST and SSS Using Frequencies in the Range 0.3–2.0ÂGHz. Radio Science, 2022, 57, .	1.6	1
3	Correcting Sea Surface Temperature Spurious Effects in Salinity Retrieved From Spaceborne L-Band Radiometer Measurements. IEEE Transactions on Geoscience and Remote Sensing, 2021, 59, 7256-7269.	6.3	23
4	Microwave Radiometry at Frequencies From 500 to 1400 MHz: An Emerging Technology for Earth Observations. IEEE Journal of Selected Topics in Applied Earth Observations and Remote Sensing, 2021, 14, 4894-4914.	4.9	16
5	Revisiting the Global Patterns of Seasonal Cycle in Sea Surface Salinity. Journal of Geophysical Research: Oceans, 2021, 126, e2020JC016789.	2.6	13
6	Seawater Debye Model Function at L-Band and Its Impact on Salinity Retrieval From Aquarius Satellite Data. IEEE Transactions on Geoscience and Remote Sensing, 2021, 59, 8103-8116.	6.3	21
7	Lessons Learned from SMAP Radiometer Pre-/Post-launch Calibration. , 2021, , .		0
8	Spurious Signal in SMAP Fourth Stokes Parameter. IEEE Transactions on Geoscience and Remote Sensing, 2021, 59, 9472-9485.	6.3	0
9	Soil Moisture Active/Passive (SMAP) L-Band Microwave Radiometer Post-Launch Calibration Revisit: Approach and Performance. IEEE Journal of Selected Topics in Applied Earth Observations and Remote Sensing, 2021, 14, 11406-11416.	4.9	2
10	Spaceâ€Based Observations for Understanding Changes in the Arcticâ€Boreal Zone. Reviews of Geophysics, 2020, 58, e2019RG000652.	23.0	39
11	The Multifrequency Future for Remote Sensing of Sea Surface Salinity from Space. Remote Sensing, 2020, 12, 1381.	4.0	17
12	Sea surface salinity estimates from spaceborne L-band radiometers: An overview of the first decade of observation (2010–2019). Remote Sensing of Environment, 2020, 242, 111769.	11.0	120
13	Reference-Quality Emission and Backscatter Modeling for the Ocean. Bulletin of the American Meteorological Society, 2020, 101, E1593-E1601.	3.3	10
14	Smap Microwave Radiometer Calibration Revisit Approaches and Performamnce. , 2020, , .		0
15	Debye Dielectric Model Function for Seawater Based on Expanded L-Band Measurement Data Set. , 2020, , .		0
16	Editorial for the Special Issue "Sea Surface Salinity Remote Sensing― Remote Sensing, 2019, 11, 1300.	4.0	1
17	Soil Moisture Active/Passive (SMAP) L-Band Microwave Radiometer Post-Launch Calibration Upgrade. IEEE Journal of Selected Topics in Applied Earth Observations and Remote Sensing, 2019, 12, 1647-1657.	4.9	14
18	Sea Surface Salinity Distribution in the Southern Ocean as Observed From Space. Journal of Geophysical Research: Oceans, 2019, 124, 3186-3205.	2.6	10

EMMANUEL DINNAT

#	Article	IF	CITATIONS
19	Remote Sensing of Sea Surface Salinity: Comparison of Satellite and In Situ Observations and Impact of Retrieval Parameters. Remote Sensing, 2019, 11, 750.	4.0	55
20	L-Band Seawater Dielectric Model Function Based on Improved Measurement Data Set. , 2019, , .		1
21	Sea Surface Salinity Retrievals from Aquarius Using Neural Networks. , 2019, , .		1
22	Satellite Sea Surface Salinity: Evaluation of Products and Impact of Retrieval Algorithms. , 2019, , .		1
23	A Theoretical Algorithm for the Retrieval of Sea Surface Salinity from Smap Observations. , 2019, , .		Ο
24	SMAP Observations of the Fourth Stokes Parameter At L-Band. , 2019, , .		2
25	Status of Aquarius and Salinity Continuity. Remote Sensing, 2018, 10, 1585.	4.0	20
26	Smap Microwave Radiometer: Instrument Status and Calibration for the First Three Years of Operation. , 2018, , .		2
27	Emissivity of Frozen Regions Retrieved from Aquarius Measurements. , 2018, , .		Ο
28	Seawater Dielectric Measurements at L-Band with Latest Improvements. , 2018, , .		3
29	Aquarius Final Release Product and Full Range Calibration of L-Band Radiometers. , 2018, , .		Ο
30	Intercalibration of Low Frequency Brightness Temperature Measurements For Long-Term Soil Moisture Record. , 2018, , .		2
31	L-, C- and X-Band Passive Microwave Soil Moisture Retrieval Algorithm Parameterization Using in Situ Validation Sites. , 2018, , .		2
32	Status of Aquarius Salinity. , 2018, , .		1
33	Soil Moisture Active/Passive L-Band Microwave Radiometer Postlaunch Calibration. IEEE Transactions on Geoscience and Remote Sensing, 2017, 55, 5339-5354.	6.3	18
34	Improved Sea Ice Fraction Characterization for L-Band Observations by the Aquarius Radiometers. IEEE Transactions on Geoscience and Remote Sensing, 2017, 55, 1285-1304.	6.3	12
35	Satellite observed salinity distributions at high latitudes in the <scp>N</scp> orthern <scp>H</scp> emisphere: A comparison of four products. Journal of Geophysical Research: Oceans, 2017, 122, 7717-7736.	2.6	33
36	Sea surface salinity: Inter-comparison of satellite products, in situ measurements, and impact of differences in retrieval algorithm. , 2017, , .		1

Emmanuel Dinnat

#	Article	IF	CITATIONS
37	Improved ICE fraction model for I-band remote sensing. , 2017, , .		Ο
38	L-Band Model Function of the Dielectric Constant of Seawater. IEEE Transactions on Geoscience and Remote Sensing, 2017, 55, 6964-6974.	6.3	28
39	Dielectric constant measurements for remote sensing of seawater salinity. , 2017, , .		0
40	ReCalibration and validation of the SMAP L-band radiometer. , 2017, , .		1
41	Intercomparison of brightness temperature measurements from SMAP and SMOS radiometers. , 2017, , .		1
42	The dielectric constant model function and implications for remote sensing of salinity. , 2017, , .		1
43	Multi-frequency radiometer-based soil moisture retrieval algorithm parametrization using in situ validation sites. , 2017, , .		2
44	Status of aquarius and the salinity retrieval. , 2016, , .		1
45	L-band radiometer calibration consistency assessment for the SMOS, SMAP and Aquarius instruments. , 2016, , .		1
46	Calibration and validation of the SMAP L-band radiometer. , 2016, , .		1
47	Recent improvements in L-band observations of ocean salinity by aquarius. , 2016, , .		0
48	Satellite and In Situ Salinity: Understanding Near-Surface Stratification and Subfootprint Variability. Bulletin of the American Meteorological Society, 2016, 97, 1391-1407.	3.3	126
49	Roughness and foam signature on SMOS-MIRAS brightness temperatures: A semi-theoretical approach. Remote Sensing of Environment, 2016, 180, 221-233.	11.0	32
50	Status of Aquarius/SAC-D and Aquarius Salinity Retrievals. IEEE Journal of Selected Topics in Applied Earth Observations and Remote Sensing, 2015, 8, 5401-5415.	4.9	34
51	Aquarius L-band Radiometers Calibration Using Cold Sky Observations. IEEE Journal of Selected Topics in Applied Earth Observations and Remote Sensing, 2015, 8, 5433-5449.	4.9	17
52	Assessing Long-Term Stability of SMOS Zero-Baseline Antenna Temperature Using the Aquarius Antenna Temperature Simulator. IEEE Geoscience and Remote Sensing Letters, 2015, 12, 1680-1684.	3.1	3
53	The impact of the assimilation of Aquarius sea surface salinity data in the GEOS ocean data assimilation system. Journal of Geophysical Research: Oceans, 2014, 119, 6974-6987.	2.6	23
54	Weekly gridded Aquarius L-band radiometer/scatterometer observations and salinity retrievals over the polar regions – Part 2: Initial product analysis. Cryosphere, 2014, 8, 915-930.	3.9	26

2

#	Article	IF	CITATIONS
55	Weekly gridded Aquarius L-band radiometer/scatterometer observations and salinity retrievals over the polar regions – Part 1: Product description. Cryosphere, 2014, 8, 905-913.	3.9	18
56	Comparison of SMOS and Aquarius Sea Surface Salinity and analysis of possible causes for the differences. , 2014, , .		1
57	Aquarius radiometer status. , 2014, , .		Ο
58	Effect of Snow Surface Metamorphism on Aquarius L-Band Radiometer Observations at Dome C, Antarctica. IEEE Transactions on Geoscience and Remote Sensing, 2014, 52, 7408-7417.	6.3	23
59	Inter-comparison of SMOS and aquarius Sea Surface Salinity: Effects of the dielectric constant and vicarious calibration. , 2014, , .		12
60	Advances in calibration of the SMOS zero-baseline radiometers. , 2014, , .		0
61	Aquarius whole range calibration: Celestial Sky, ocean, and land targets. , 2014, , .		7
62	Activeâ€passive synergy for interpreting ocean Lâ€band emissivity: Results from the CAROLS airborne campaigns. Journal of Geophysical Research: Oceans, 2014, 119, 4940-4957.	2.6	10
63	Aquarius: Status and recent results. Radio Science, 2014, 49, 709-720.	1.6	13
64	Aquarius overview and up date. , 2014, , .		0
65	Aquarius Third Stokes Parameter Measurements: Initial Results. IEEE Geoscience and Remote Sensing Letters, 2013, 10, 520-524.	3.1	20
66	Aquarius RFI detection and mitigation. , 2013, , .		0
67	Synthesizing SMOS zero-baselines with Aquarius brightness temperature simulator. , 2012, , .		Ο
68	Comparison of aquarius measurements over oceans with radiative transfer models at L-band. , 2012, , .		0
69	Comparison of Aquarius measurements and radiative transfer models at L-band. , 2012, , .		4
70	Impact of Antenna Pattern on Measurement of the Third Stokes Parameter From Space at L-Band. IEEE Transactions on Geoscience and Remote Sensing, 2011, 49, 406-414.	6.3	15
71	The Aquarius Simulator and Cold-Sky Calibration. IEEE Transactions on Geoscience and Remote Sensing, 2011, 49, 3198-3210.	6.3	38

72 Background emissions during cold sky calibration of Aquarius. , 2010, , .

Emmanuel Dinnat

#	Article	IF	CITATIONS
73	Spurious signal in measurement of the third Stokes parameter from space at L-band. , 2010, , .		0
74	Effect of Emission From the Moon on Remote Sensing of Sea Surface Salinity: An Example With the Aquarius Radiometer. IEEE Geoscience and Remote Sensing Letters, 2009, 6, 239-243.	3.1	8
75	Impact of Sun Glint on Salinity Remote Sensing: An Example With the Aquarius Radiometer. IEEE Transactions on Geoscience and Remote Sensing, 2008, 46, 3137-3150.	6.3	26
76	L-band radiometry and reflection of the galaxy by a rough ocean surface. , 2008, , .		3
77	Sun glint and sea surface salinity remote sensing. , 2007, , .		0
78	The influence of antenna pattern on Faraday rotation in remote sensing at L-band. , 2007, , .		2
79	Effects of the Antenna Aperture on Remote Sensing of Sea Surface Salinity at L-Band. IEEE Transactions on Geoscience and Remote Sensing, 2007, 45, 2051-2060.	6.3	20
80	The Influence of Antenna Pattern on Faraday Rotation in Remote Sensing at L-Band. IEEE Transactions on Geoscience and Remote Sensing, 2007, 45, 2737-2746.	6.3	29
81	Aquarius Mission Technical Overview. , 2006, , .		16
82	Surface emission. , 2006, , 225-426.		3
83	Absolute Calibration of Radar Altimeters: Consistency with Electromagnetic Modeling. Journal of Atmospheric and Oceanic Technology, 2005, 22, 771-781.	1.3	7
84	Wind speed effect on L-band brightness temperature inferred from EuroSTARRS and WISE 2001 field experiments. IEEE Transactions on Geoscience and Remote Sensing, 2004, 42, 2206-2213.	6.3	38
85	Ionospheric Effects for L-Band 2-D Interferometric Radiometry. IEEE Transactions on Geoscience and Remote Sensing, 2004, 42, 105-118.	6.3	14
86	Surface Salinity Retrieved from SMOS Measurements over the Global Ocean: Imprecisions Due to Sea Surface Roughness and Temperature Uncertainties. Journal of Atmospheric and Oceanic Technology, 2004, 21, 1432-1447.	1.3	50
87	Issues concerning the sea emissivity modeling at L band for retrieving surface salinity. Radio Science, 2003, 38, n/a-n/a.	1.6	70
88	Influence of sea surface emissivity model parameters at L-band for the estimation of salinity. International Journal of Remote Sensing, 2002, 23, 5117-5122.	2.9	42
89	Effects of the Antenna Aperture on Remote Sensing of Sea Surface Salinity at L-band , 0, , .		1